https://doi.org/10.5194/egusphere-2026-2356
Preprint. Discussion started: 30 April 2026

Meteoroids as a source of metal ion clouds in Earth's upper thermosphere

Gang Chen[1]*, Yimeng Xu[1], Guotao Yang[2]*, Wuhu Feng[3], Jiyao Xu[2], Shaodong Zhang[1,4], Guozhu Li[5], Hanxian Fang[6], Lifang Du[2], Haoran Zheng[2], Xuewu Cheng[7], Faquan Li[7], Yuchang Xun[8], Kaiming Huang[1], Chunxiao Yan[2]

[1] School of Earth and Space Science and Technology, Wuhan University, Wuhan, 430072, China

[2] National Space Science Center, Chinese Academy of Sciences, Beijing, 100190, China

[3] School of Chemistry, University of Leeds, Leeds, UK

[4] School of Physics and Electronic Science, Guizhou Normal University, Guiyang, 550025, China

[5] Institute of Geology and Geophysics, Chinese Academy of Sciences, Beijing, 100029, China

[6] College of Advanced Interdisciplinary Studies, National University of Defense Technology, Changsha, 410073, China

[7] Innovation Academy for Precision Measurement Science and Technology, Chinese Academy of Sciences, Wuhan, 430071, China

[8] College of Physics and Optoelectronics, Taiyuan University of Technology, Taiyuan 030024, China

Corresponding Author: Gang Chen (g.chen@whu.edu.cn) and Guotao Yang (gtyang@nssc.ac.cn)

Abstract. Advances in lidar technology have enabled the detection of Metal Ion Clouds (MICs) at altitudes between 120-300 km in the Earth's thermosphere. Observations from a Ca^+ lidar in Beijing, China, reveal that these MICs are characterized by tightly packed, stripe-like structures that span extensive areas, covering hundreds to thousands of square kilometers. Some of these stripes extend downward to the Main Metal Layer (MML) around 100 km, and some clouds descend with tidal winds and merge into the underlying MML. While arriving the altitudes of Mesosphere and Low-Thermosphere (MLT), they lead to an increase in Sporadic-E (Es) layer density, and even trigger the formation of a new Es layer. The metal ions in the upper thermosphere will eventually sink into the MML and significantly affect its density variations. The striped structure of MICs and their direct

https://doi.org/10.5194/egusphere-2026-2356
Preprint. Discussion started: 30 April 2026

effects on Es and MML suggest they originate from meteoroid trails, challenging traditional views on meteoric input.

1 Introduction

The thermosphere is a layer of Earth's atmosphere situate between the mesosphere below and the exosphere above (Walker, 1988). It begins at approximately 90 km and extends upward to an altitude of 500 km, sometimes reaching as high as 1000 km. In the lower thermosphere, the predominant neutral species are molecular nitrogen (N_2) and molecular oxygen (O_2). Throughout this region, the most abundant neutrals are atomic oxygen (O), N_2, and O_2. Solar high-energy X-ray and ultraviolet radiation ionize atoms and molecules in this layer, producing ions such as NO^+ and O^+, which in turn form the ionosphere (Torr, 1983; Kopp & Herrmann, 1984).

Metallic elements in Earth's atmosphere are highly concentrated in the Mesosphere and Lower Thermosphere (MLT) region at altitudes between 80-105 km, where atmospheric density increases dramatically. When meteoroids enter this region, intense heat from friction with atmospheric gases melts and evaporates their surface. This process leads to the release of metal atoms and ions from the meteoroids. These released elements such as Fe, Mg, Na, K, Ca, and Ni, form the well-known metal layer in the MLT region (Qian and Gardner, 1995; Plane et al., 2012, 2015). The structures and variations of the atomic and ionic layers within this metal layer have been extensively and deeply studied (e.g., Granier et al., 1985; Gardner et al., 1993; Gerding et al., 2000; Chu et al., 2011, 2020, 2021).

Our understanding of metallic elements in the upper thermosphere and ionospheric F-layer above the metal layer remains quite limited. Unlike non-metal species, the abundance of metallic elements in this altitude range is extremely low, and observational techniques for detecting them are severely constrained. Rocket and satellite payloads have proven to be effective means of measurement (e.g., Broadfoot et al., 1967; Hanson and Sanatani, 1971; Grebowsky and Brinton, 1978; Gardner et al., 1999). Based on such in-situ observations, it is generally accepted that metals in the upper thermosphere originate from two primary sources. During daytime, the eastward electric field at the magnetic equator lifts metal ions from the metal layer to sufficiently high altitudes via E×B drift; these ions then spread poleward along geomagnetic field lines into low-latitude regions (e.g., Carter and

https://doi.org/10.5194/egusphere-2026-2356
Preprint. Discussion started: 30 April 2026

Forbes, 1999; Hanson et al., 1972). At high latitudes, strong polar electric fields can directly transport metal ions upward to greater heights (e.g., Bristow and Watkins, 1991; Nygrén et al., 1984; Chu & Yu, 2017). However, there is no direct observational evidence to support the mechanisms described above.

With advances in technology, the sensitivity of lidar systems has continued to improve. In recent years, the Ca^+ lidar located in Yanqing, Beijing, China has extended its observational range from the MLT region up to 300 km in the upper thermosphere (Jiao et al., 2022). On many nights, cloud-like structures composed of Ca^+ have been detected between 120-300 km altitude, with durations exceeding 5 hours. The observations have revealed many intriguing characteristics of the Metal Ion Clouds (MICs) in terms of spatial distribution and temporal evolution, offering a perspective on their origin that differs from earlier understanding. The underlying mechanisms challenge existing explanations and may reshape several conventional concepts in space physics and meteor astronomy, paving the way for fundamentally new interpretations of well- known phenomena.

2 Observation Instruments

The resonance-fluorescence dual-wavelength lidar located in Yanqing, Beijing, China (40.4°N, 116.0°E) is an all-solid-state narrowband system designed for the observation of neutral Ca and Ca^+. This lidar is operated by the National Space Science Center of the Chinese Academy of Sciences. Its transmitter, receiver, data- acquisition system, and technical parameters have been described in detail in earlier work (Wu et al., 2020). In March 2020, the original two broadband pulsed dye lasers were replaced with two solid-state, injection-seeded, pulsed Optical Parametric Oscillator (OPO) lasers. The per-pulse laser output was increased from 9 mJ to 30 mJ, and the repetition rate was changed from 30 Hz to 15 Hz. Compared with conventional dye-based lidars, the OPO technology offers higher pulse energy, narrower bandwidth, and superior beam quality (Du et al., 2023), which substantially improves the photon-return signal. From June 2020 to December 2022, the Ca^+ lidar operated with a time resolution of 33 s and a height resolution of 96 m.

The Digisonde located in Changping (40.3°N, 116.2°E) is produced by the Lowell Digisonde International and operated by the Institute of Geology and Geophysics, Chinese Academy of Sciences (Reinisch et al., 2009). It transmits radio waves vertically in steps of 50 kHz across the 1-14 MHz frequency range and records the reflected echoes to produce an ionogram every 15 minutes. The

https://doi.org/10.5194/egusphere-2026-2356
Preprint. Discussion started: 30 April 2026

recorded echo virtual height extends from 80 km to 1360 km with a height resolution of 2.5 km. Key ionospheric parameters, such as the critical frequency of sporadic-E (foEs), the critical frequency of the F-layer (foF2), and the virtual height of the F-layer (h'F2), are derived directly from these ionograms.

Total Electron Content (TEC) is obtained from the time delay between the two transmitted frequencies of Global Navigation Satellite System (GNSS) signals. Only data with an inclined signal path below 30° are used, and the ionospheric pierce point is set at 250 km altitude. The observations come from a network of 260 GNSS receivers distributed across the Chinese mainland. The TEC data are provided by the Crustal Movement Observation Network of China (CMONOC) with a time resolution of 30 s (Wang, 2016).

The Fabry-Perot Interferometer (FPI) at Xinglong, Hebei Province, China (40.2°N, 117.4°E) is part of the Chinese Meridian Project (Wang, 2010; Wang et al., 2024). It measures night airglow emissions at OH 892.0 nm (peak altitude ~87 km), OI 557.7 nm (~97 km), and OI 630.0 nm (~250 km) in the vertical direction and along four oblique look directions. From these measurements, three-dimensional wind velocities at the three corresponding altitudes are derived with a time resolution of one hour (Yuan et al., 2010).

3 Results

3.1 Metal Ions in Upper Thermosphere

https://doi.org/10.5194/egusphere-2026-2356
Preprint. Discussion started: 30 April 2026

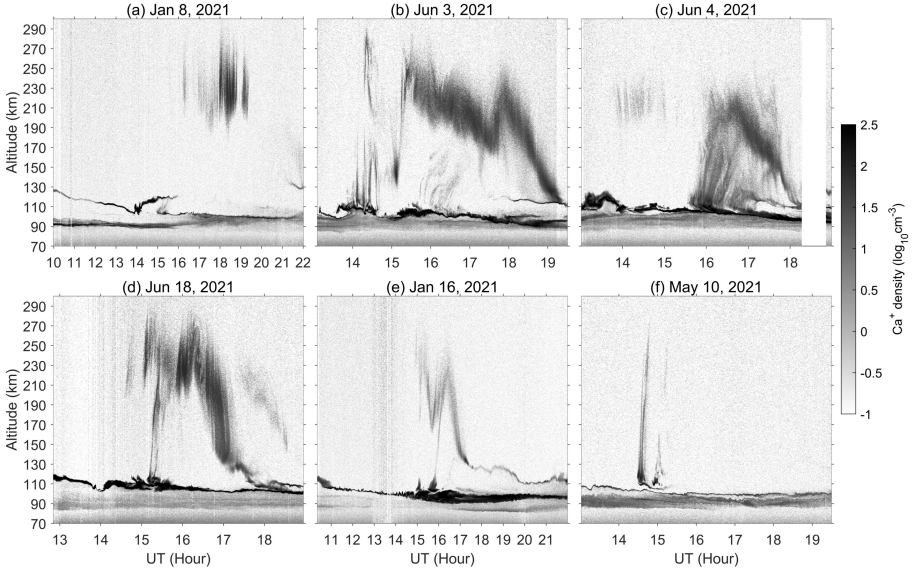

Figure 1. Ca^+ variations between 70-300 km altitude. Observations from the Ca^+ lidar are presented for (a) January 8, 2021, (b) June 3, 2021, (c) June 4, 2021, (d) June 18, 2021, (e) January 16, 2022, and (f) May 10, 2021. LT = UT + 8 hr. The main metal layer is typically located between 80 km and 120 km altitude, while the metal ion clouds frequently occur between 120 km and 300 km.

Between June 2020 and October 2022, the Ca^+ lidar at Yanqing, Beijing, China (40.4°N, 116.0°E) was successfully operated on 257 nights. Ca^+ structures above 150 km altitude were recorded on 37 of those nights, with clearly defined layers between 200-300 km observed on 15 nights. Six representative cases from 8 and 16 January, 10 May, 3, 4 and 18 June 2021 are displayed in Figure 1. The data are publicly available on Zenodo (Xu & Chen, 2025). The observed Ca^+ is distributed in two distinct regions: the MLT region and the upper thermosphere. The dense, layered structure between 80-120 km altitude corresponds to the Main Metal Layer (MML), which is detectable throughout the night in the MLT region. The other form consists of much lower- density MICs, which occasionally appear in the upper thermosphere between 120-300 km.

MICs sometimes exist independently in the upper thermosphere without any apparent connection to the underlying MML. Examples include the structures between 190-290 km in Figure 1a, those between 190 -250 km from 13:44 to 15:06 UT in Figure 1c, and the descending feature from 230 km down to 130 km between 17:30-18:30 UT in Figure 1d. In other cases, MICs are visibly linked to the MML. One type of connection appears as straight, stripe-like structures that directly bridge the two,

https://doi.org/10.5194/egusphere-2026-2356
Preprint. Discussion started: 30 April 2026

such as those seen during 14:00-14:30 UT in Figure 1b, 15:32-17:10 UT in Figure 1c, at 15:16 UT in Figure 1d, at 15:43 UT in Figure 1e, and at 14:35 UT in Figure 1f. Another type involves slowly descending clouds that eventually merge into the MML, as observed at 19:00 UT in Figure 1b, 18:00 UT in Figure 1c, and 17:30 UT in Figure 1d. In these events, metal ions descend gradually with tidal winds. Upon reaching the MLT region, wind shear compresses them into thin layers- a process analogous to the behavior of intermediate tidal ion layers that form between the ionospheric E and F regions, detach from the bottom side of the F layer, and descend to merge into the sporadic-E (Es) layer (Mathews, 1998; Chen et al., 2024; Yu et al., 2021).

Close inspection reveals that all MICs in the upper thermosphere share a common morphology: they are composed of narrow, well-defined stripes. Most stripes are parallel to each other, although non-parallel alignments also occur, as seen in Figure 1e. As noted earlier, some stripes extend downward to ~100 km altitude, establishing a direct connection with the MML.

3.2 Total Electron Content Enhancement

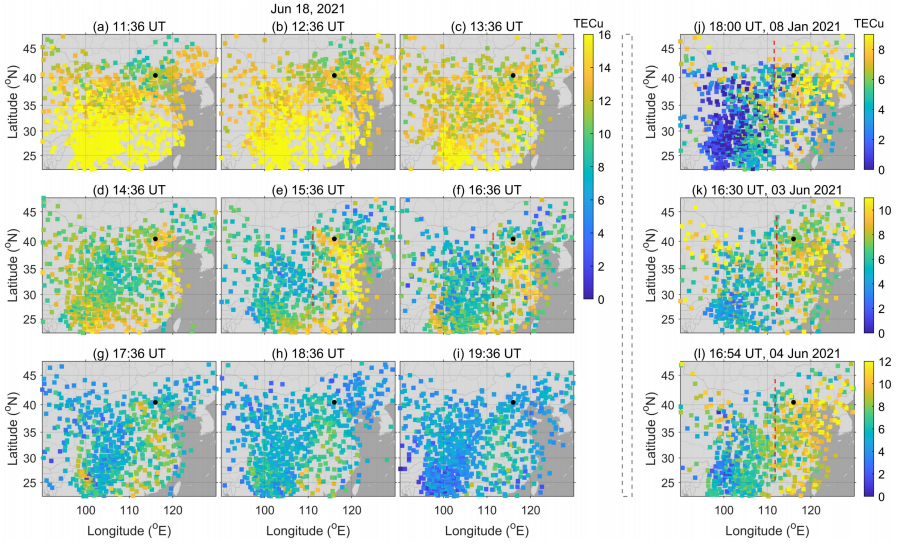

Figure 2. Two-dimension Total Electron Content (TEC) maps. (a-i) Time sequence of TEC maps from 12:18 to 19:36 UT on 18 June 2021. (j-l) TEC maps at 18:00 UT on 8 January, 16:30 UT on 3 June, and 16:54 UT on 4 June 2021, respectively. The black dot marks the location of the lidar; the red vertical dashed line indicates the region of enhanced TEC on the right side.

https://doi.org/10.5194/egusphere-2026-2356
Preprint. Discussion started: 30 April 2026

MICs occur at altitudes corresponding to the ionospheric F-layer- do they influence this layer? The evidence suggests they do. When Ca^+ clouds were observed in the upper thermosphere, spread-F frequently appeared in ionograms (Figure 3), and regional enhancements in Total Electron Content (TEC) were simultaneously recorded by the GNSS network. TEC data are publicly available on Zenodo (Xu & Chen, 2025). Example TEC maps for 8 January, 3, 4 and 18 June 2021 are shown in Figure 2. A time sequence from 12:18 to 19:36 UT (20:18-03:36 LT) on 18 June (Figures 2a-2i) illustrates the typical evolution: after sunset, as recombination gradually exceeds photoionization, TEC values generally decline. However, a regional TEC enhancement emerged above the lidar site at 14:36 UT (Figure 2d), coinciding with the onset of MIC detection in Figure 1d. The enhanced region, marked by the red vertical line in Figures 2e and 2f, extended southward from about 42° N to 25° N. By 17:36 UT (Figure 2g), the enhancement had weakened considerably and had nearly vanished by 19:36 UT (Fig. 2i). Notably, the MIC also disappeared from the lidar field of view after 18:30 UT, indicating a close temporal correspondence between the MIC presence and the TEC enhancement.

Similar meridionally extended TEC enhancements were recorded during MIC observations on 8 January and 3-4 June 2021 (Figures 2j-2l). The spatial scale of these enhancements- often covering hundreds to thousands of square kilometers- suggests that the corresponding ion clouds are extensive, consistent with their persistence over several hours in the lidar observations (Figure 1). Although localized plasma density increases are not uncommon in the nighttime F-region, no concurrent disturbances in the wind field or electric field were identified that could account for these TEC enhancements during the MIC events.

3.3 Correlation between MIC and Es

Es layer is a thin, irregular region of high plasma density that occur sporadically at altitudes between 90-120 km and are composed primarily of metal ions. Figure 3 examines variations of Es layer when MICs were connected to the MML. The gray bars in Figures 3a-3e show the critical frequency of Es (foEs) variations from 13:00 to 20:00 UT on 3, 4 and 18 June, 16 January, and 10 May 2021, respectively; no bar is plotted when Es was absent. As noted earlier, the MICs in Figure 1 exhibited two distinct types of connections to the MML. When they extended almost directly downward to the MML, their duration is marked with a red dashed box. When they descended slowly toward the MML, a blue

https://doi.org/10.5194/egusphere-2026-2356
Preprint. Discussion started: 30 April 2026

vertical line indicates the onset of merging. In every case, foEs increased during these connection events, signaling a rise in ion density.

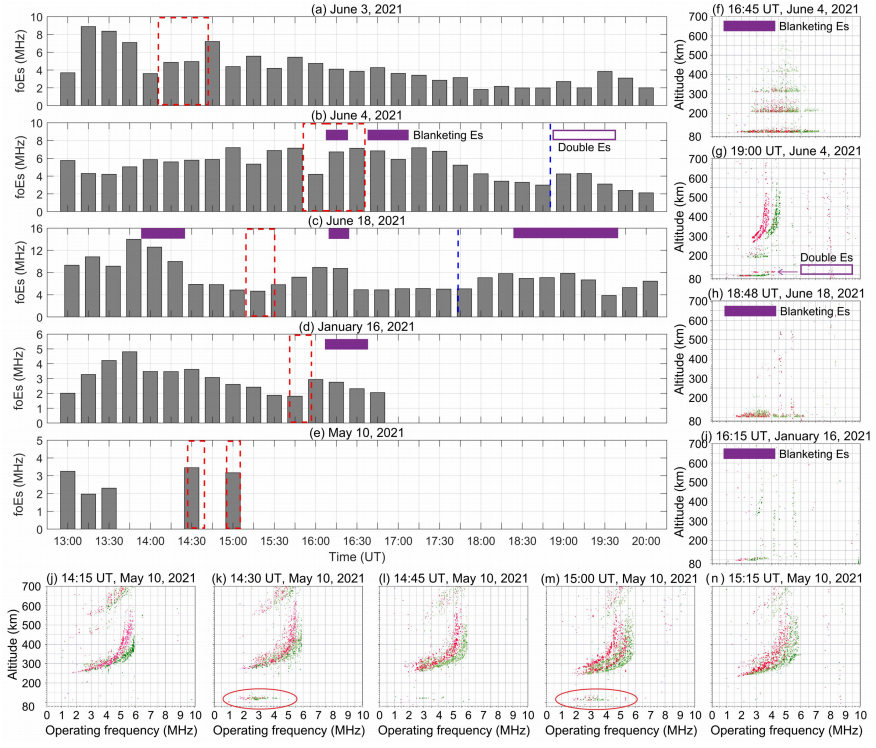

Figure 3. Observations of the Digisonde in Beijing. (a-e) Temporal variations in the critical frequency of the Es layer (f_oEs) on 3 June, 4 June, 18 June, 16 January, and 10 May 2021. The red dashed box marks the period during which stripe-like structures extend directly downward to the main metal layer. Blue vertical lines indicate the onset of descending metal ion clouds merging into the main metal layer. The solid purple square and purple box denote the durations of blanketing Es and double Es, respectively. (f-n) Example ionograms recorded by the Digisonde in Beijing. The red ovals highlight the suddenly appearing Es.

On certain occasions, blanketing Es (indicated by solid purple squares) occurred during or shortly after the connection events. Es layer typically exhibits a patchy structure, allowing radio waves to pass through the gaps and reach the higher F-region; thus, Es is usually semitransparent. However, as seen in the ionograms in Figures 3f, 3h, and 3i, blanketing Es- characterized by dense ionization- completely obscured the upper ionospheric layers in Digisonde observations. Moreover, after 18:50 UT on 4 June,

https://doi.org/10.5194/egusphere-2026-2356
Preprint. Discussion started: 30 April 2026

the MIC in Figure 1c had descended to about 110 km and was compressed into a thin layer; a double metal layer was then observed. The ionogram in Figure 3g confirms that the upper component of this double Es layer was also located near 110 km.

The most striking sequence occurred on 10 May (Figure 3e). After 13:00 UT, the Es layer disappeared. However, when elongated Ca^+ stripes extended from the upper thermosphere down to ~110 km at 14:30 and 15:00 UT in Figure 1f, an Es layer suddenly reappeared at 110 km in the ionograms (Figures 3k and 3m). The time series of ionograms presented in the bottom row highlights this remarkable correspondence between the Ca^+ stripes and the resurgence of the Es layer. Furthermore, following the first stripe structure in Figure 1f, a new metal layer formed beneath it and persisted until 15:20 UT.

All the above phenomena indicate that MICs supply metal ions to the MLT region through these connecting structures.

3.4 Correlation between MIC and MML

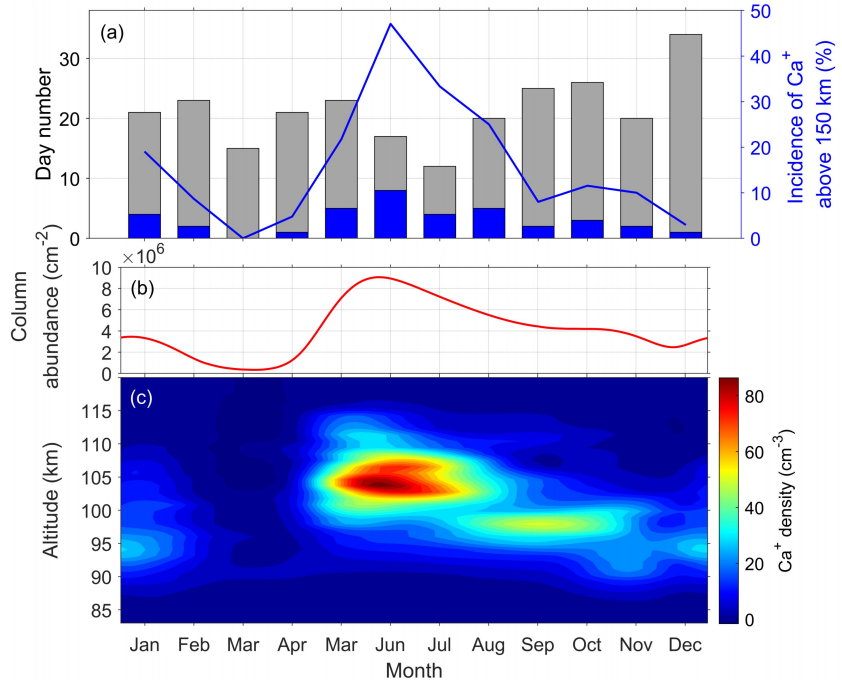

Figure 4. Comparison of Ca^+ in the upper thermosphere and the MLT region. (a) The gray and blue

https://doi.org/10.5194/egusphere-2026-2356
Preprint. Discussion started: 30 April 2026

histograms represent the total number of observational days per month from 2020 to 2022 and the number of days with Ca^+ detected above 150 km altitude, respectively. The blue curve shows the occurrence rate of Ca^+ above 150 km. (b) Monthly average of the Ca^+ column density between 83 km and 120 km altitude. (c) Monthly average of the Ca^+ number density between 83 km and 120 km altitude.

The preceding analysis suggests that metal ions originating from MICs can intensify Es layers and may even generate new ones. A natural follow-up question is: what influence do MICs exert on the MML, which resides at altitudes similar to those of Es?

Figure 4 presents statistical results of Ca^+ recorded by the lidar. The Ca^+ dataset is publicly available on Zenodo (Xu & Chen, 2025). The gray bars in Figure 4a show the monthly number of observation days over the three-year period. The blue bars represent the monthly count of nights on which Ca^+ structures were detected above 150 km. No such events were recorded in March, while only one event was identified in each of April and December. In contrast, four or more events were recorded in January, May, June, July, and August. The occurrence rate of Ca^+ above 150 km, plotted as the blue curve in Figure 4a, peaks markedly in June and the adjacent months, with a secondary, smaller peak in January.

The annual variation of Ca^+ number density between 83-120 km is shown in Figure 4c. The average Ca^+ density in May, June, and July is significantly higher than in other months. The red curve in Figure 4b illustrates the variation in Ca^+ column density, i.e., the height-integrated Ca^+ density. Column density is considerably elevated from May to August relative to other months, and is also higher in January than in the surrounding months, with the lowest value occurring in March. This red curve closely matches the blue occurrence-rate curve in Figure 4a, indicating a strong positive correlation between Ca^+ observed above 150 km and Ca^+ within the underlying MML.

Based on the above analysis of the observational data, we conclude that metal ions present in the upper thermosphere eventually converge into the metal layer in the MLT region and significantly influence its density variations.

3.5 Fine Structure of MIC

The morphology of these MICs is particularly striking. Rather than forming continuous structures, they consist of distinct, closely spaced stripes. These stripes occur between 110-290 km altitude, with

https://doi.org/10.5194/egusphere-2026-2356
Preprint. Discussion started: 30 April 2026

222 vertical extents ranging from tens to hundreds of kilometers. Most stripes are nearly straight, with little
223 curvature, and such striped formations have not been previously reported in the thermosphere or
224 ionospheric F-region. As demonstrated in Figure 3, when these stripes extend downward into the MLT
225 region, they deliver a substantial amount of metal ions that enhance the density of the Es layer and can
226 even trigger the formation of a new Es layer.

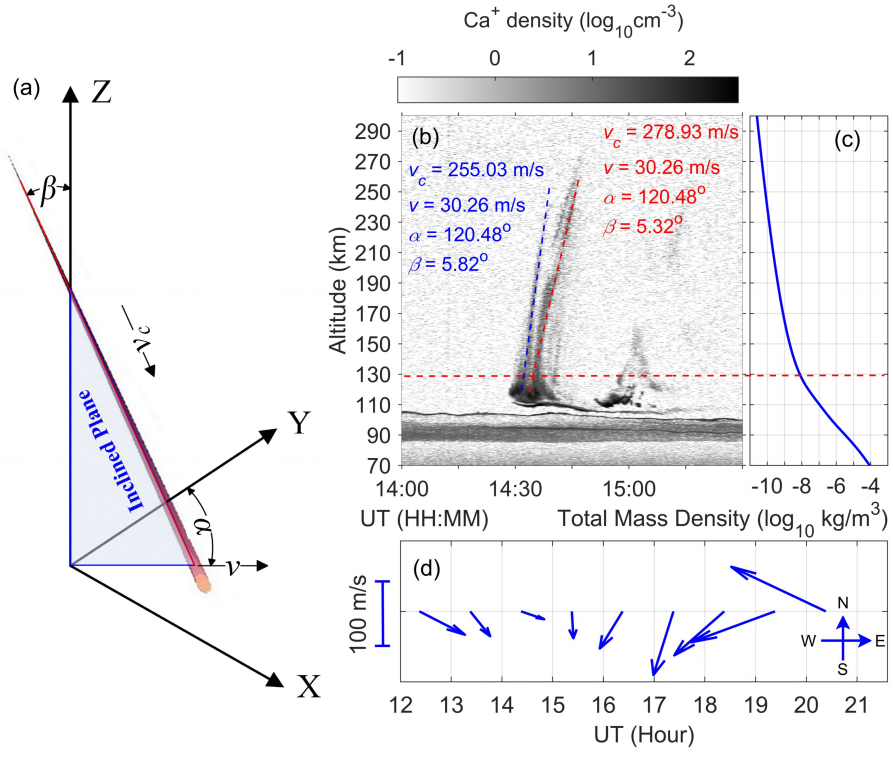

227

228 **Figure 5. Case study of metal ion stripes. (a) Spatial parameters of a typical metal ion stripe. (b) Enlarged**
229 **view of Fig. 1f, with the two marked stripes labeled by blue and red dashed lines and their corresponding**
230 **spatial parameters indicated. (c) Vertical atmospheric density profile above the lidar site at 14:30 UT. (d)**
231 **Variation of the horizontal wind field at 250 km altitude measured by the FPI at Xinglong.**

232 The stripes in Figure 1f extend from ~260 km down to 110 km and exerted a clear influence on
233 the Es layer. To examine them in detail, we show an enlarged view of these stripes around 14:30 UT in
234 Figure 5b. The two stripes of interest are marked with blue and red dashed lines. As altitude decreases,
235 the stripes broaden. Below 130 km- indicated by the red horizontal line- their density and width
236 increase abruptly, eventually forming a thin, dense layer near 110 km altitude. This behavior is

https://doi.org/10.5194/egusphere-2026-2356
Preprint. Discussion started: 30 April 2026

characteristic of metal ion stripes; the long descending stripes in Figures 1c-1f exhibit the same pattern.

The blue curve in Figure 5c presents the vertical atmospheric density profile above the lidar site at 14:30 UT, derived from the NRLMSISE-00 model. Atmospheric density rises sharply with decreasing altitude, increasing by two orders of magnitude below 130 km. This correspondence indicates that the morphology of the stripes is governed by atmospheric density, and the abrupt rise in density below 130 km likely drives the enhanced production of metal ions. The dataset of horizontal wind field at 250 km is publicly available on Zenodo (Xu & Chen, 2025).

4 Discussion

Consider a riddle: Something flies straight through Earth's atmosphere at tremendous speed, and rapidly descends. Upon reaching the MLT region- where air density increases abruptly- it releases large amounts of metal ions, forming a metal ion layer or an Es layer. The answer, of course, is a meteoroid.

Meteoroids enter Earth's atmosphere at speeds ranging from 11 to 72 km s^{-1} (Plane et al., 2015). As they encounter the denser atmosphere in the MLT region, aerodynamic heating causes their surfaces to vaporize, releasing abundant metal atoms and ions into the air (Ceplecha et al., 1998). This heating also ionizes and excites the surrounding gas, producing the luminous phenomenon known as a meteor. Optical cameras can capture meteors and estimate their trajectories; their luminous trails typically start between 80-90 km altitude. High-power radars can detect meteor head echoes up to about 120 km (Chau et al., 2007, 2014; Zhou et al., 2001). While lidar cannot directly track the meteoroid itself, it can detect the metal ions left behind, effectively revealing the ionized trails. Owing to its high sensitivity, the lidar used in this study can observe such trails even at very high altitudes. We therefore propose that the tight stripes composing the MICs may be formed by the ionized trails of numerous meteoroids belonging to the same shower.

The zenith angles of the some stripe structures of the MICs can be estimated. The lidar beam is very narrow and points vertically upward, making it rare to capture a long meteoroid trail. As illustrated in Figure 5a, a long stripe is recorded only when the trail moves within its inclined plane and crosses the lidar beam. The larger the angle between the inclined plane and the horizontal motion direction v of the trail, the shorter the detected metal-ion stripe. Therefore, when a long stripe (>80 km) is observed, the corresponding meteoroid trail must be moving nearly within its inclined plane.

https://doi.org/10.5194/egusphere-2026-2356
Preprint. Discussion started: 30 April 2026

Observations from Peru indicate that nighttime zonal plasma drift velocities correlate well with zonal neutral winds (Chapagain et al., 2013). Because meridional plasma motions are only weakly influenced by E×B forcing, horizontal plasma drift velocities can also be expected to correlate with horizontal neutral winds. Hence, the horizontal wind velocity measured by the Fabry-Perot interferometer (FPI) in Beijing at 250 km altitude (Figure 2d) can, to some extent, represent the horizontal motion of the trail. The wind-field dataset is available via the Zenodo website (Xu and Chen, 2025). The zenith angle β of the meteoroid trail can then be approximated from the slope of the stripe v_c and the horizontal velocity v:

$$\beta = \arctan(v/v_c) \quad (1)$$

For the two Ca^+ stripes marked in Figure 5b, the derived β values are 5.82° and 5.32°, respectively. All measured stripes yield β values ranging from 0.21° to 49.07°. Meteoroids belonging to the same shower typically originate from fragments of the same cometary dust and therefore enter Earth's atmosphere on nearly parallel paths- consistent with the predominantly parallel alignment of the observed trails.

According to conventional ablation theory, when a meteoroid descends into the MLT region, the ambient gas density becomes sufficient to cause intense aerodynamic heating, liberating surface atoms through thermal processes (Ceplecha et al., 1998). The altitude range over which significant ablation occurs depends on the meteoroid's physical properties and its atmospheric entry velocity (Ceplecha, 1968). Meteoroids with low melting points or exceptionally high speeds can undergo ablation at altitudes above 130 km. During certain meteor showers, long meteor trails have been observed at heights up to 400 km (Brosch et al., 2001; Fujiwara et al., 1998). It is particularly noteworthy that Broadfoot et al. (1967) reported detecting Ca^+ at altitudes extending from 100 to 280 km, and the observed increase in meteor activity suggests that this emission originated from meteor trails at these heights. To explain meteoroid ionization in the tenuous atmosphere of the upper thermosphere, the sputtering theory has been proposed (Guttormsen et al., 2020; Rogers et al., 2005). Sputtering refers to the direct ejection of particles from a meteoroid surface due to high-speed atomic collisions.

https://doi.org/10.5194/egusphere-2026-2356
Preprint. Discussion started: 30 April 2026

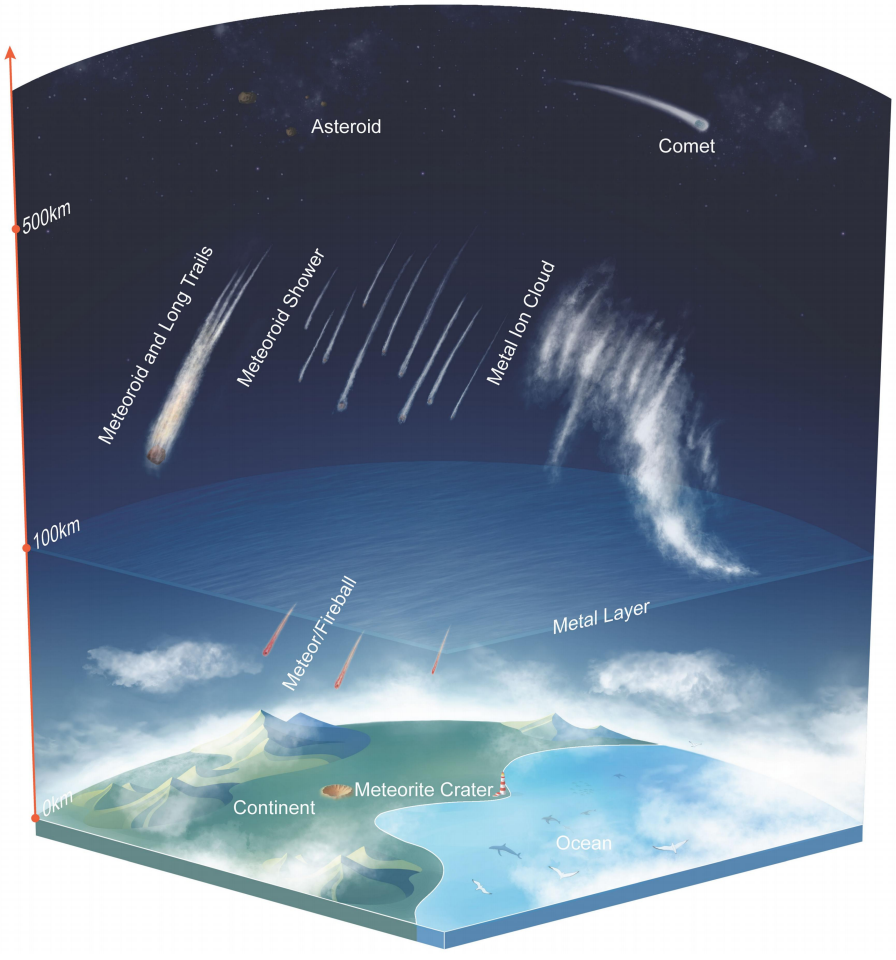

Figure 6. Schematic of metal ion cloud formation. The main metal layer is centered near 100 km altitude. Bright meteors (fireballs) typically ablate below this layer, while the observed metal ion clouds form above it, as a result of meteoroid ablation in the upper thermosphere.

Based on the preceding analysis and discussion, Figure 6 schematically illustrates the formation of MICs in the upper thermosphere. Luminous meteors and their plasma trails commonly occur below the MML, where gas density is high enough to produce sufficient frictional heating. In contrast, a little has been known until now about metallic elements in the thermosphere above the MML.

Our measurements reveal that MICs reside between 120-300 km altitude, consist of tightly packed stripes, and can extend over thousands of square kilometers. The consistent striped morphology indicates that this structure is intrinsic to MICs and not a later artifact. As depicted in Figure 6, longer

https://doi.org/10.5194/egusphere-2026-2356
Preprint. Discussion started: 30 April 2026

trails originate from larger meteoroids that penetrate to the MML before ablating completely, whereas an MIC itself is composed of numerous such trails from a meteoroid shower. Metal ions in the thermosphere have longer lifetimes than molecular ions and do not disappear rapidly through recombination. They descend with tidal winds and are eventually captured by wind shear in the MLT region, thereby merging into and reinforcing the MML.

5 Conclusion

We report evidence for extensive Metal Ion Clouds (MICs) in the upper thermosphere (120-300 km) revealed by high-sensitivity Ca^+ lidar observations. These MICs exhibit a distinctive morphology- dense ensembles of narrow, quasi-parallel stripes- spanning hundreds to thousands of square kilometres and persisting for hours. Crucially, the MICs in the upper thermosphere constitute a substantial, previously underappreciated reservoir that ultimately feeds the mesospheric metal system.

MICs likely comprise numerous ionized meteoroid trails produced during shower activity, extending to much higher altitudes than implied by conventional views based on optical meteor onset heights. It suggests that meteoroid-atmosphere interaction and metal injection can operate efficiently in the rarefied upper thermosphere, with consequences that propagate downward through atmospheric dynamics and ion-neutral coupling.

By identifying MICs as a large-scale, structured source of metals in the upper atmosphere and linking them to measurable ionospheric responses, this work reframes how meteoric input should be incorporated into models of the thermosphere-ionosphere system. The findings motivate coordinated observations and modelling across meteor astronomy, upper-atmosphere chemistry, and space physics to quantify the metal budget, determine the controlling microphysical processes at high altitude, and assess the implications for space-weather variability and radio-wave propagation.

Data Availability Statement. The data of metal atoms, FPI and TEC can be publicly obtained in the Zenodo website (https://doi.org/10.5281/zenodo.15713532) (Xu & Chen, 2025).

Author contributions. G.C. performed the analysis, investigated the physical mechanisms and wrote the manuscript. Y.X. from Wuhan University conducted data analysis and plotted the data. G.Y. is the

https://doi.org/10.5194/egusphere-2026-2356
Preprint. Discussion started: 30 April 2026

person in charge of the Ca^+ lidar and implemented the lidar observation. W.F. analyszed the lidar observation resultes and suggestted the posibility of meteoroid ablation. G.L. provided the digisonde data. J.X. is the person in charge of the FPI and provided the wind field data. L.D., H.Z., X.C., and F.L. carried out the lidar observation in Bejing for three years and organized the datasets. S.Z. and H.F. discussed the influence of the metal ions on atmosphere. Y.X. from Taiyuan University of Technology assisted in Ca^+ seasonal variation processing. K.H. and C.Y. analyzed the impact of the metal ions on ionosphere.

Conflict of Interest Disclosure. The contact author has declared that none of the authors has any competing interests.

Acknowledgments. This project was supported by the National Natural Science Foundation of China (42274197). We acknowledge the use of the lidar data and FPI data from the Chinese Meridian Project. The digisonde data were provided by Beijing National Observatory of Space Environment, Institute of Geology and Geophysics Chinese Academy of Sciences through the Geophysics center, National Earth System Science Data Center. We acknowledge Professor Fan Yi from Wuhan University for the valuable suggestions of the meteor sputtering in the upper thermosphere. Gang Chen and Yimeng Xu are co-first authors.

Reference

Bristow, W. A., & Watkins, B. J.: Numerical simulation of the formation of thin ionization layers at high latitudes. Geophysical Research Letters, 18(3), 404–407. https://doi.org/10.1029/90GL02588, 1991.

Brosch, N., Schijvarg, L. S., Podolak, M., & Rosenkrantz, M. R.: Meteor observations from Israel. In B. Warmbein (Ed.), Proceedings of the Meteoroids 2001 Conference, (pp. 165–173). Kiruna, Sweden. 2001.

Broadfoot, A. L.: Twilight Ca^+ emission from meteor trails up to 280 km. Planetary and Space Science, 15(3), 503–514. https://doi.org/10.1016/0032-0633(67)90159-6, 1967.

https://doi.org/10.5194/egusphere-2026-2356
Preprint. Discussion started: 30 April 2026

353 Carter, L. N., & Forbes, J. M.: Global transport and localized layering of metallic ions in the upper
354 atmosphere. Annales Geophysicae, 17, 190–209. https://doi.org/10.1007/s00585-999-0190-6,
355 1999.
356 Ceplecha, Z.: Discrete levels of meteor beginning height. Smithsonian Astrophysical Observatory
357 Special Report, 279. 1968.
358 Ceplecha, Z., Borovička, J., Elford, W. G., Revelle, D. O., Hawkes, R. L., Porubčan, V., & Šimek, M.:
359 Meteor phenomena and bodies. Space Science Reviews, 84, 327–471.
360 https://doi.org/10.1023/A:1005069928850, 1998.
361 Chapagain, N. P., Fisher, D. J., Meriwether, J. W., Chau, J. L., & Makela, J. J.: Comparison of zonal
362 neutral winds with equatorial plasma bubble and plasma drift velocities. Journal of Geophysical
363 Research: Space Physics, 118(4), 1802–1812. https://doi.org/10.1002/jgra.50238, 2013.
364 Chau, J. L., Woodman, R. F., & Galindo, F.: Sporadic meteor sources as observed by the Jicamarca
365 high-power large-aperture VHF radar. Icarus, 188(1), 162–174.
366 https://doi.org/10.1016/j.icarus.2006.11.006, 2007.
367 Chau, J. L., Strelnikova, I., Schult, C., Oppenheim, M. M., Kelley, M. C., Stober, G., & Singer, W.:
368 Nonspecular meteor trails from non-field-aligned irregularities: Can they be explained by presence
369 of charged meteor dust? Geophysical Research Letters, 41(10), 3336–3343.
370 https://doi.org/10.1002/2014GL059922, 2014.
371 Chen, G. et al.: Intermediate descending layers emerged simultaneously in five different locations
372 during the solar eclipse on 21 June 2020. Journal of Geophysical Research: Space Physics, 129(7),
373 e2023JA032340. https://doi.org/10.1029/2023JA032340, 2024.
374 Chu, X., Yu, Z., Gardner, C. S., Chen, C., & Fong, W.: Lidar observations of neutral Fe layers and fast
375 gravity waves in the thermosphere (110–155 km) at McMurdo, Antarctica. Geophysical Research
376 Letters, 38(23), L23807. https://doi.org/10.1029/2011GL050016, 2011.
377 Chu, X., & Yu, Z.: Formation mechanisms of neutral Fe layers in the thermosphere at Antarctica
378 studied with a thermosphere–ionosphere Fe/Fe^+ model. Journal of Geophysical Research: Space
379 Physics, 122(6), 6812–6848. https://doi.org/10.1002/2016JA023773, 2017.
380 Chu, X., Nishimura, Y., Xu, Z., Yu, Z., Plane, J. M. C., Gardner, C. S., & Ogawa, Y.: First simultaneous
381 lidar observations of thermosphere-ionosphere Fe and Na (TIFe and TINa) layers at McMurdo
382 (77.84°S, 166.67°E), Antarctica with concurrent measurements of aurora activity, enhanced

https://doi.org/10.5194/egusphere-2026-2356
Preprint. Discussion started: 30 April 2026

ionization layers, and converging electric field. Geophysical Research Letters, 47, e2020GL090181. https://doi.org/10.1029/2020GL090181, 2020.

Chu, X. et al.: Mid-latitude thermosphere–ionosphere Na (TINa) layers observed with high-sensitivity Na Doppler lidar over Boulder (40.13°N, 105.24°W). Geophysical Research Letters, 48(11), e2021GL093729. https://doi.org/10.1029/2021GL093729, 2021.

Du, L. et al.: The all-solid-state narrowband lidar developed by optical parametric oscillator/amplifier technology for simultaneous detection of the Ca and Ca^+ layers. Remote Sensing, 15(18), 4566. https://doi.org/10.3390/rs15184566, 2023.

Fujiwara, Y., Ueda, M., Sugimoto, T., Kinoshita, K., Shimoda, M., & Nakamura, A.: Meteor luminosity at 160 km altitude from TV observations for bright Leonid meteors. Geophysical Research Letters, 25(3), 285–288. https://doi.org/10.1029/97GL03766, 1998.

Gardner, C. S., Kane, T. J., Senft, D. C., Qian, J., & Papen, G. C.: Simultaneous observations of sporadic E, Na, Fe, and Ca^+ layers at Urbana, Illinois: Three case studies. Journal of Geophysical Research: Space Physics, 98(D9), 16865–16873. https://doi.org/10.1029/93JD01477, 1993.

Gardner, J. A., Broadfoot, A. L., McNeil, W. J., Lai, S. T., & Murad, E.: Analysis and modeling of the GLO-1 observations of meteoric metals in the thermosphere. Journal of Atmospheric and Solar-Terrestrial Physics, 61(7), 545–562. https://doi.org/10.1016/S1364-6826(99)00013-9, 1999.

Gerding, M., Alpers, M., von Zahn, U., Rollason, R. J., & Plane, J. M. C.: Atmospheric Ca and Ca^+ layers: Midlatitude observations and modeling. Journal of Geophysical Research: Space Physics, 105(A12), 27131–27146. https://doi.org/10.1029/2000JA900088, 2000.

Granier, G., Jégou, J. P., & Mégie, G.: Resonant lidar detection of Ca and Ca^+ in the upper atmosphere. Geophysical Research Letters, 12(10), 655–658. https://doi.org/10.1029/GL012i010p00655, 1985.

Grebowsky, J. M., & Brinton, H. C.: Fe^+ ions in the high-latitude F region. Geophysical Research Letters, 5(9), 791–794. https://doi.org/10.1029/GL005i009p00791, 1978.

Guttormsen, G., Fletcher, A. C., & Oppenheim, M. M.: Atomic-scale simulations of meteor ablation. Journal of Geophysical Research: Space Physics, 125(9), e2020JA028229. https://doi.org/10.1029/2020JA028229, 2020.

Hanson, W. B., & Sanatani, S.: Relationship between Fe^+ ions and equatorial spread F. Journal of Geophysical Research, 76(31), 7761–7768. https://doi.org/10.1029/JA076i031p07761, 1971.

https://doi.org/10.5194/egusphere-2026-2356
Preprint. Discussion started: 30 April 2026

412 Hanson, W. B., Sterling, D. L., & Woodman, R. F.: Source and identification of heavy ions in the
413 equatorial F layer. Journal of Geophysical Research, 77(28), 5530–5541.
414 https://doi.org/10.1029/JA077i028p05530, 1972.
415 Jiao, J. et al.: First lidar profiling of meteoric Ca^+ ion transport from ~ 80 to 300 km in the midlatitude
416 nighttime ionosphere. Geophysical Research Letters, 49, e2022GL100537.
417 https://doi.org/10.1029/2022GL100537, 2022.
418 Kopp, E., & Herrmann, U. R.: Ion composition in the lower ionosphere. Annales Geophysicae, 2(1),
419 83–94. 1984.
420 Mathews, J. D.: Sporadic E: Current views and recent progress. Journal of Atmospheric and
421 Solar-Terrestrial Physics, 60(4), 413–435. https://doi.org/10.1016/S1364-6826(97)00043-6, 1998.
422 Nygrén, T., Jalonen, L., Oksman, J., & Turunen, T.: The role of electric field and neutral wind direction
423 in the formation of sporadic E layers. Journal of Atmospheric and Terrestrial Physics, 46(4),
424 373–381. https://doi.org/10.1016/0021-9169(84)90122-3, 1984.
425 Plane, J. M. C.: Cosmic dust in the Earth's atmosphere. Chemical Society Reviews, 41(19), 6507–6518.
426 https://doi.org/10.1039/C2CS35132C, 2012.
427 Plane, J. M. C., Feng, W., & Dawkins, E. C. M.: The mesosphere and metals: Chemistry and changes.
428 Chemical Reviews, 115(10), 4497–4541. https://doi.org/10.1021/cr500501m, 2015.
429 Qian, J., & Gardner, C. S.: Simultaneous lidar measurements of mesospheric Ca, Na, and temperature
430 profiles at Urbana, Illinois. Journal of Geophysical Research: Atmospheres, 100(D4), 7453–7461.
431 https://doi.org/10.1029/94JD02748, 1995.
432 Reinisch, B. W. et al.: New digisonde for research and monitoring applications. Radio Science, 44(1),
433 RS0A24. https://doi.org/10.1029/2008RS004115, 2009.
434 Rogers, L. A., Hill, K. A., & Hawkes, R. L.: Mass loss due to sputtering and thermal processes in
435 meteoroid ablation. Planetary and Space Science, 53(13), 1341–1354.
436 https://doi.org/10.1016/j.pss.2005.07.002, 2005.
437 Torr, D. G.: Neutral and ion composition of the thermosphere. Reviews of Geophysics, 21(2), 245–262.
438 https://doi.org/10.1029/RG021i002p00245, 1983.
439 Walker, J. C. G.: The mid-latitude thermosphere. Planetary and Space Science, 36(1), 1–10.
440 https://doi.org/10.1016/0032-0633(88)90141-9, 1988.

https://doi.org/10.5194/egusphere-2026-2356
Preprint. Discussion started: 30 April 2026

441 Wang, C.: New chains of space weather monitoring stations in China. Space Weather, 8(8).
442 https://doi.org/10.1029/2010SW000603, 2010.
443 Wang, C.: Comparison of ionospheric characteristic parameters obtained by GPS and ionosonde with
444 IRI model over China. Journal of Earth System Science, 125, 745–759.
445 https://doi.org/10.1007/s12040-016-0694-x, 2016.
446 Wang, C., Xu, J., Chen, Z., Li, H., Feng, X., Huang, Z., & Wang, J.: China's ground-based space
447 environment monitoring network-Chinese Meridian Project (CMP). Space Weather, 22(7),
448 e2024SW003972. https://doi.org/10.1029/2024SW003972, 2024.
449 Wu, F. et al.: Simultaneous detection of the Ca and Ca^+ layers by a dual-wavelength tunable lidar
450 system. Applied Optics, 59(13), 4122–4130. https://doi.org/10.1364/AO.381699, 2020.
451 Xu, Y., & Chen, G.: Metal ion clouds composed by the dense meteoroid trails in middle thermosphere
452 [Data set]. Zenodo. https://doi.org/10.5281/zenodo.15713532, 2025.
453 Yuan, W. et al.: First observation of mesospheric and thermospheric winds by a Fabry–Perot
454 interferometer in China. Chinese Science Bulletin, 55, 4046–4051.
455 https://doi.org/10.1007/s11434-010-4192-2, 2010.
456 Yu, B. et al.: Interhemispheric transport of metallic ions within ionospheric sporadic E layers by the
457 lower thermospheric meridional circulation. Atmospheric Chemistry and Physics, 21, 4219–4230.
458 https://doi.org/10.5194/acp-21-4219-2021, 2021.
459 Zhou, Q. H., Mathews, J. D., & Nakamura, T.: Implications of meteor observations by the MU radar.
460 Geophysical Research Letters, 28(7), 1399–1402. https://doi.org/10.1029/2000GL012504, 2001.